

## Fluorescence

Rational Molecular Design towards Vis/NIR Absorption and Fluorescence by using Pyrrolopyrrole *aza*-BODIPY and its Highly Conjugated Structures for Organic Photovoltaics\*\*Soji Shimizu,<sup>\*,[a]</sup> Taku Iino,<sup>[b]</sup> Akinori Saeki,<sup>\*,[c]</sup> Shu Seki,<sup>[c]</sup> and Nagao Kobayashi<sup>\*,[b]</sup>

**Abstract:** Pyrrolopyrrole *aza*-BODIPY (PPAB) developed in our recent study from diketopyrrolopyrrole by titanium tetrachloride-mediated Schiff-base formation reaction with heteroaromatic amines is a highly potential chromophore due to its intense absorption and fluorescence in the visible region and high fluorescence quantum yield, which is greater than 0.8. To control the absorption and fluorescence of PPAB, particularly in the near-infrared (NIR) region, further molecular design was performed using DFT calculations. This results in the postulation that the HOMO–LUMO gap of PPAB is perturbed by the heteroaromatic moieties and the aryl-substituents. Based on this molecular design, a series of new PPAB molecules was synthesized, in which the largest

redshifts of the absorption and fluorescence maxima up to 803 and 850 nm, respectively, were achieved for a PPAB consisting of benzothiazole rings and terthienyl substituents. In contrast to the sharp absorption of PPAB, a PPAB dimer, which was prepared by a cross-coupling reaction of PPAB monomers, exhibited panchromatic absorption across the UV/Vis/NIR regions. With this series of PPAB chromophores in hand, a potential application of PPAB as an optoelectronic material was investigated. After identifying a suitable PPAB molecule for application in organic photovoltaic cells based on evaluation using time-resolved microwave conductivity measurements, a maximized power conversion efficiency of 1.27% was achieved.

## Introduction

Creation of functional chromophore molecules, whose optical properties can be controlled by simple derivatization such as introduction of substituents or replacement of part of the structure has recently become increasingly important, due to the potential utilization of these types of chromophore molecules in the fields of bio-imaging, electroluminescence, photochemical sensing, and organic photovoltaics.<sup>[1,2]</sup> Diketopyrrolopyrrole (DPP)<sup>[3–5]</sup> is a fascinating bicyclic lactam, widely utilized in industry as a red colorant. In recent years, this unique molecule has been focused on as an optoelectronic material due to its excellent photophysical properties such as photostability and intense absorption in the visible region.<sup>[6]</sup> Although chemi-

cal modification of the ketone moieties of DPP has great potential for extension of the conjugated systems to create new functional chromophore molecules, most of the previous efforts have been devoted to chemical modification of the aryl substituents on DPP by using cross-coupling reactions to fabricate donor–acceptor small molecules or polymers for application in organic photovoltaics.<sup>[6,7]</sup> In addition, another reason for this lies in the inherent low reactivity of the carbonyl carbon atoms towards nucleophilic substitution reactions, which was pointed out in the initial research on DPP by Iqbal et al.<sup>[4a,b]</sup> Only two examples of nucleophilic substitution reactions had been reported before the recent pioneering study by Zumbusch and Daltrozzi. Both of the nucleophilic substituted products were synthesized through activation of the ketone moiety with phosphorous pentasulfide (P<sub>4</sub>S<sub>10</sub>) or phosphoryl chloride (POCl<sub>3</sub>) into a thioketone species or a mono-phosphorylated species.<sup>[4a,b]</sup> Zumbusch et al. further developed the latter method to extend the conjugated systems through methine carbons to the heteroaromatic ring units and finally converted DPP into new pyrrolopyrrole-bridged dimeric boron dipyrromethene (BODIPY) analogues, which they referred to as pyrrolopyrrole cyanines.<sup>[8]</sup> Recently we found that titanium tetrachloride-mediated Schiff-base formation reaction can provide another new route for nucleophilic substitution reactions of DPP and successfully synthesized dimeric *aza*-BODIPY analogues 1–3, which are referred to as pyrrolopyrrole *aza*-BODIPY (PPAB).<sup>[9,10]</sup>

PPAB exhibited intense absorption and fluorescence with fluorescence quantum yields of over 0.8. The gradual redshift

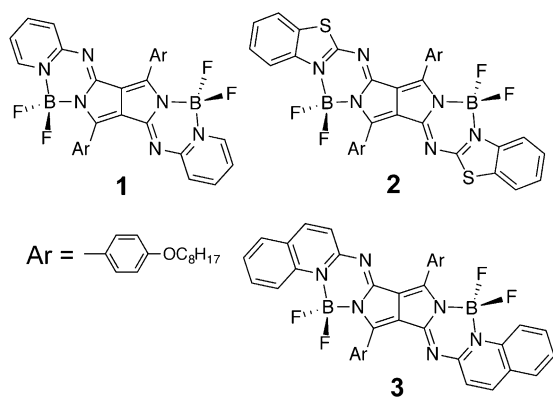
[a] Prof. Dr. S. Shimizu  
Department of Chemistry and Biochemistry  
Graduate School of Engineering, Kyushu University  
Fukuoka 819-0395 (Japan)  
E-mail: ssoji@cstf.kyushu-u.ac.jp

[b] T. Iino, Prof. Dr. N. Kobayashi  
Department of Chemistry, Graduate School of Science  
Tohoku University, Sendai 980-8578 (Japan)  
E-mail: nagaok@m.tohoku.ac.jp

[c] Prof. Dr. A. Saeki, Prof. Dr. S. Seki  
Department of Applied Chemistry, Graduate School of Engineering  
Osaka University, Suita, 565-0871 (Japan)  
E-mail: saeki@chem.eng.osaka-u.ac.jp

[\*\*] BODIPY = boron dipyrromethene.

Supporting information for this article is available on the WWW under <http://dx.doi.org/10.1002/chem.201405761>.



of the absorption and fluorescence observed in the order from **1** to **2** and to **3** was indicative of significant perturbation of the electronic structure of PPAB by the heteroaromatic ring moieties. Striking structural difference of PPAB from pyrrolopyrrole cyanines<sup>[8]</sup> is the high co-planarity of the phenyl-substituents on the pyrrolopyrrole moiety with respect to the PPAB core structure, which is due to the lower steric hindrance of the imine bridging compared to the methine carbon bridges with cyano-substituents in the structures of pyrrolopyrrole cyanines. This structural feature implies non-negligible substituent effects on the optical properties of PPAB. Changes in both the heteroaromatic ring units and substituents on the pyrrolopyrrole moiety can, therefore, be utilized to control the absorption and fluorescence of PPAB molecules. In this study, shift of the absorption and fluorescence even further into the near infrared (NIR) region was successfully achieved through survey of potential combinations of the heteroaromatic ring units and types of substituent based on the DFT and time-dependent DFT (TDDFT) calculations.

In the course of the synthesis of PPAB with various aryl substituents on the pyrrolopyrrole moiety using cross-coupling reactions, we envisioned extension of the conjugated system of this chromophore by dimerization. Under the conditions of palladium-catalyzed borylation and in situ cross-coupling reaction, a dimer of PPAB can be easily synthesized. Surprisingly, this compound exhibited panchromatic absorption across the UV/Vis/NIR regions.

In this manuscript, the synthesis and molecular design of these new PPAB molecules and their intriguing optical properties are described. In addition, with this series of compounds in hand, their application as optoelectronic materials in organic photovoltaics with bulk heterojunction architectures was also investigated. After optimization of the solubility of PPAB and the device fabrication conditions based on an electrochemical study on PPAB molecules and time-resolved microwave photoconductivity measurements using white-light pulse,<sup>[11]</sup> a promising performance as the first application of these compounds in organic photovoltaics was achieved.

## Results and Discussion

### Molecular design based on DFT and TDDFT calculations

The PPAB molecules **1–3**<sup>[9]</sup> exhibited intriguingly intense absorption and fluoresce in the lower-energy visible region (**1**:  $\lambda_{\text{abs}}=638$  nm,  $\lambda_{\text{em}}=661$  nm, **2**:  $\lambda_{\text{abs}}=655$  nm,  $\lambda_{\text{em}}=672$  nm, **3**:  $\lambda_{\text{abs}}=671$  nm,  $\lambda_{\text{em}}=692$  nm ( $\lambda_{\text{abs}}$  and  $\lambda_{\text{em}}$  denote absorption and fluorescence maxima)). The fluorescence quantum yields of these compounds were exceptionally high (**1**:  $\Phi_{\text{F}}=0.87$ , **2**:  $\Phi_{\text{F}}=0.81$ , **3**:  $\Phi_{\text{F}}=0.83$ ). Since a redshift of fluorescence is in general accompanied by a significant decrease in the fluorescence quantum yield, which is one of the reasons why NIR fluorophores have remained very limited, it is a reasonable strategy to modify highly fluorescent compounds in the visible region and shift their fluorescence into the NIR region. In this sense, PPAB appears to have high potential. The TDDFT calculations (B3LYP/6-31G(d)) performed in the previous study of PPAB demonstrated that the main absorption of the PPAB molecules arises from a  $\pi\text{--}\pi^*$  transition between the highest occupied molecular orbital (HOMO) and the lowest unoccupied molecular orbital (LUMO).<sup>[9]</sup> The redshift of the main absorption from **1** to **2** and further to **3** was well reproduced based on the TDDFT calculations (**1**: 580 nm, **2**: 600 nm, **3**: 613 nm), and the calculated HOMO–LUMO energy gap ( $\Delta\text{H–L}$ ) decreased in this order (**1**: 2.20 eV, **2**: 2.16 eV, **3**: 2.10 eV). Although the transition energies were overestimated, relative shift of the absorption caused by modification of the PPAB chromophore systems can be qualitatively estimated based on DFT and TDDFT calculations at the B3LYP/6-31G(d) level.

To shift the absorption and fluorescence of PPAB to the NIR region, we envisioned the modification of two potential components in the PPAB structure: 1) Heteroaromatic ring moieties and 2) Substituents on the pyrrolopyrrole moiety. The redshift caused by the former has been confirmed both in our previous study and in the study of pyrrolopyrrole cyanines by Zumbach and Daltrozzo.<sup>[8]</sup> The latter effect also appeared to be possible due to the co-planarity of the phenyl substituents with respect to the PPAB core structure with dihedral angles of 30–40° observed in the crystal structures of **1–3**.<sup>[9]</sup> In the case of pyrrolopyrrole cyanines, the substituent effect is rather marginal due to the nearly perpendicular orientation of the aryl substituents to the pyrrolopyrrole moiety caused by the steric hindrance of the cyano groups.<sup>[8h]</sup> Taking these into consideration, potential structures of PPAB for NIR absorption were surveyed by using DFT and TDDFT calculations (Figure 1 and Table 1).

Since PPAB attained a redshift and narrow  $\Delta\text{H–L}$  as the heteroaromatic moieties became polycyclic in the previous study,<sup>[9]</sup> a model structure of PPAB consisting of benzimidazole units (**M-2**) was estimated, and the theoretical absorption maximum and the  $\Delta\text{H–L}$  values were compared with those of a model structure of **2** (**M-1**). The redshift of the absorption maximum by 89 nm from **M-1** and the narrower  $\Delta\text{H–L}$  of **M-2** (1.88 eV) based on the DFT and TDDFT calculations implied that this modification is effective. Next, the substituent effect was estimated. When the phenyl substituents on the pyrrolopyrrole moiety of **M-1** was replaced with more electron-donat-

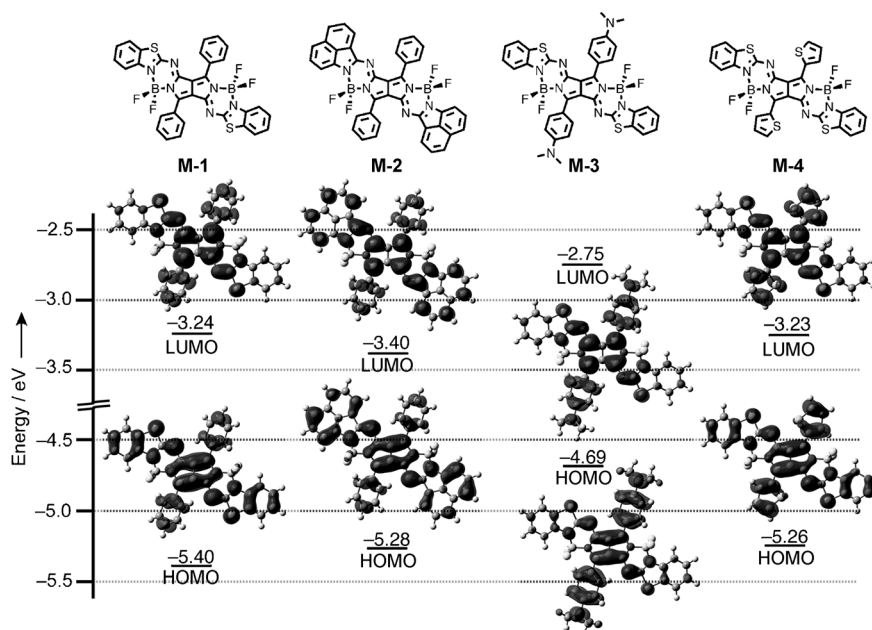


Figure 1. Frontier molecular orbitals of PPAB model structures, M-1 to M-4 (B3LYP/6-31G(d)).

Compound	HOMO [eV]	LUMO [eV]	$\Delta H-L$ [eV]	Energy [nm]	$f^{[a]}$	Wavefunction <sup>[b]</sup>
M-1	-5.40	-3.24	2.16	600	0.81	+0.711  L←H> + ...
M-2	-5.28	-3.40	1.88	689	0.97	+0.712  L←H> + ...
M-3	-4.69	-2.75	1.94	666	0.75	+0.713  L←H> + ...
M-4	-5.26	-3.23	2.03	628	0.68	+0.711  L←H> + ...

[a] Oscillator strength. [b] The wavefunctions are based on the eigenvectors predicted by TDDFT. H and L represent the HOMO and LUMO, respectively.

ing *N,N*-dimethylaminophenyl substituents (M-3) and thienyl substituents (M-4), the theoretical absorption maximum of M-1 at 600 nm shifted to 666 nm for M-3 and to 628 nm for M-4 accompanied by decrease in the  $\Delta H-L$  from 2.16 eV of M-1 to 1.94 eV of M-3 and 2.03 eV of M-4. These results also indicated effective modification of the substituents on the pyrrolopyrrole moiety towards NIR absorption.

### Synthesis and characterization

Based on the above-discussed molecular design supported by the theoretical calculations, new PPAB molecules 4–9 were synthesized (Scheme 1 and 2). Precursory DPP (DPP-1–3)<sup>[8e,12,13]</sup> and heteroaromatic amines (HA-1<sup>[14]</sup> and HA-2) were synthesized according to the literature procedures. HA-3a and HA-3b with an octyloxy substituent and a 2-hexyldecyloxy substituent at the 6-position were newly derivatized from 2-amino-6-hydroxybenzothiazole<sup>[15]</sup> in this study to attain suitable solubilities of the thienyl substituted PPAB 6a and 6b (see the Supporting Information). Due to its synthetic availability,

DPP-2 was utilized as a DPP unit with *N,N*-dialkylaminophenyl substituents. DPP and heteroaromatic amines were treated in the presence of titanium tetrachloride (TiCl<sub>4</sub>) and triethylamine in toluene under reflux,<sup>[16]</sup> followed by addition of borontrifluoride diethyl ether complex (BF<sub>3</sub>·OEt<sub>2</sub>) to provide PPAB 4, 5, 6a, and 6b in 1.0, 5.8, 39, and 30% yields, respectively. The comparatively high yields of 6a and 6b were due to the high reactivity of HA-3a and HA-3b towards DPP-3, whereas the exceptionally low yield of 4 was ascribed to the low reactivity of HA-1 towards DPP-1.

To further extend the conjugation, compound 6a was brominated with *N*-bromosuccinimide (NBS) in chloroform to form 7a, which was then converted into bithienyl and terthienyl-substituted PPAB 8 and 9 by palladium-catalyzed coupling reactions with thiophene-2-boronic acid and 5'-hexyl-2,2'-bithiophene-5-boronic acid pinacol ester.<sup>[17,18]</sup> The yields of 8 and 9 from 7a were 45 and 25%, respectively.

All these compounds were unambiguously characterized by high-resolution matrix-assisted laser desorption/ionization Fourier transform ion cyclotron resonance mass spectrometry (HR-MALDI-FT-ICR-MS) and <sup>1</sup>H NMR spectroscopy. The structure of 6b was further confirmed by X-ray single crystallographic analysis on crystals obtained from a vapor diffusion of hexane into a toluene solution of 6b (Figure 2).

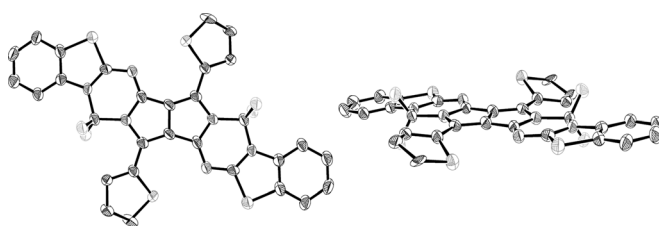
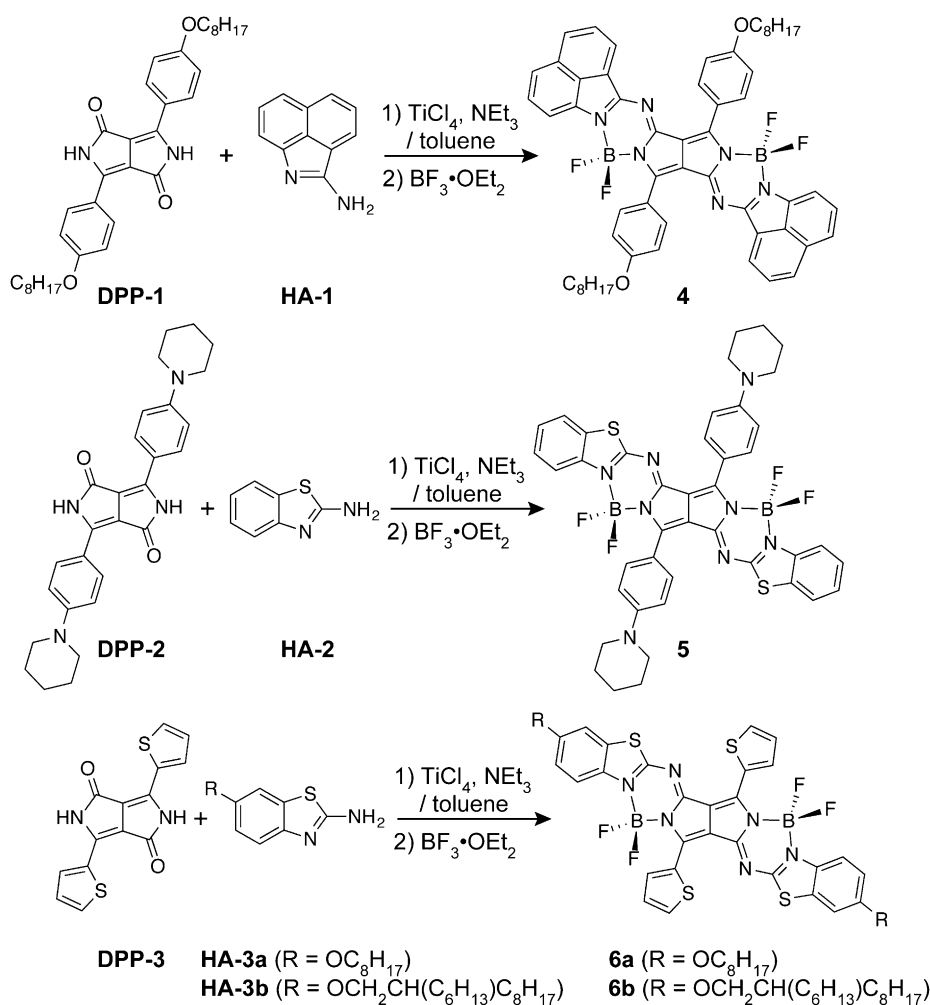


Figure 2. X-ray crystal structure of 6b, top view (left) and side view (right). The thermal ellipsoids were scaled to the 50% probability level. Hydrogen atoms, 2-hexyldecyloxy substituents, and a set of the disordered thiophene rings were omitted for clarity in both views.

In the crystal structure, the thienyl substituents were disordered into two orientations: In one orientation the sulfur atom of the thienyl substituent points towards the boron atom of the BF<sub>2</sub> unit, whereas in the other orientation it faces towards the bridging nitrogen atom. In both orientations, the dihedral angles between the thienyl substituents and the core structure of PPAB in 6b are about 27°, which is smaller than those ob-



Scheme 1. Synthesis of PPAB molecules 4–6 from DPP (DPP-1–3) and heteroaromatic amines (HA-1–3).

served for the phenyl-substituted PPAB 1–3 (30–39%)<sup>[9]</sup> due to the less bulky thienyl substituents.

### Absorption and fluorescence spectra of PPAB

All of the absorption spectra of PPAB prepared in this study exhibited similar absorption spectra, featuring an intense band and two or three following weaker bands in the shorter wavelength region, but the position of the intense band varied depending on the heteroaromatic ring moieties and substituents on the pyrrolopyrrole moiety (Figure 3a and Table 2). With respect to the absorption maximum of **2** at 655 nm, replacement of benzothiazole rings with benzoindeole rings from **2** to **4** resulted in a redshift by 92 nm. When the phenyl substituents were replaced with *p*-piperidinophenyl substituents (**5**) or thienyl substituents (**6a**), redshifts of the absorption were also observed (**5**: 733 nm, **6a**: 699 nm). In addition, compound **5** exhibited a significant broadening of the main absorption with disappearance of the shoulder absorption, whereas a new band developed at 516 nm. This band can be assigned as an intramolecular charge-transfer band, which was also reported in the case of pyrrolopyrrole cyanines with *N,N*-disubstituted

aminophenyl substituents.<sup>[8h]</sup> Upon extension of the thienyl substituents of **6a** to bithienyl (**8**) and further to terthienyl (**9**) substituents, a gradual redshift by about 50 nm per thiophene unit was observed (**8**: 756 nm, **9**: 803 nm). In the series of PPAB molecules in this study, **9** exhibited the largest redshift of the absorption, in which the tail of the absorption extended to 900 nm.

The fluorescence spectra showed a mirror-imaged emission with a Stokes shift of 159–855  $\text{cm}^{-1}$  (Figure 3b and Table 2). The fluorescence maxima also exhibited a redshift in the same order as observed for the redshift of the absorption, with the exception of **5**. The larger Stokes shift of **5** compared with the other compounds can be explained in terms of the intramolecular charge-transfer contribution. All of the compounds exhibited exceptionally high fluorescence quantum yields ( $\Phi_F$ ) relative to other conventional fluorescent compounds in the corresponding Vis/NIR regions due to the rigid

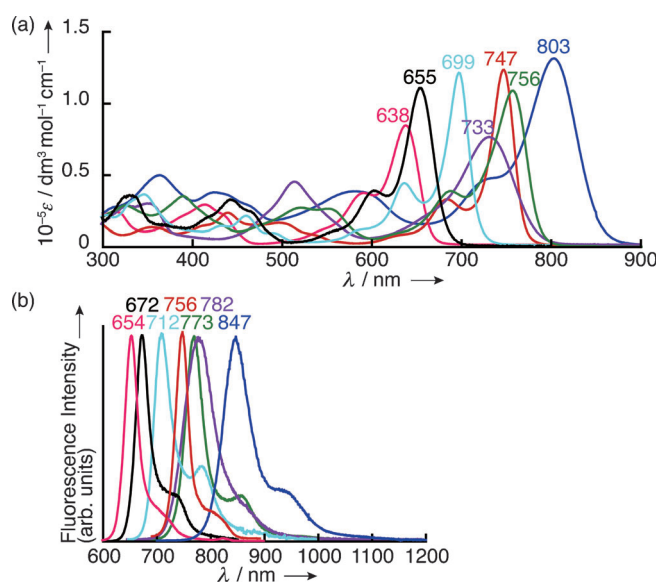
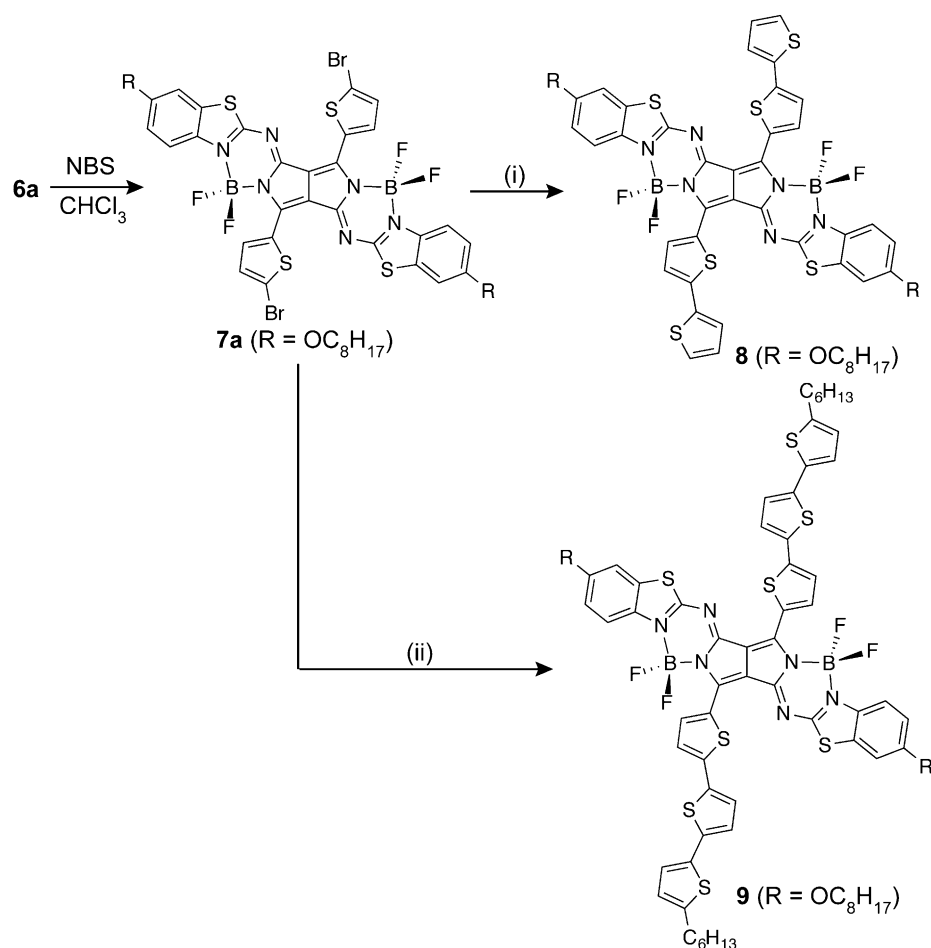


Figure 3. (a) UV/Vis/NIR absorption and (b) fluorescence spectra of PPAB molecules **4** (red), **5** (purple), **6a** (aqua blue), **8** (green), **9** (blue), and **11** (pink), in  $\text{CHCl}_3$ . UV/Vis absorption and fluorescence spectra of **2** in  $\text{CHCl}_3$  are shown as a reference (black).



**Scheme 2.** Synthesis of PPAB molecules 7–9. Reagents and conditions: (i) thiophene-2-boronic acid, [Pd(PPh<sub>3</sub>)<sub>4</sub>], Na<sub>2</sub>CO<sub>3</sub>, Aliquat336, toluene, water, reflux, 1 h; (ii) 5'-hexyl-2,2'-bithiophene-5-boronic acid pinacol ester, [PdCl<sub>2</sub>(dppf)], KOAc, DMF, 80 °C, 15 min.

**Table 2.** Summary of optical properties of PPAB molecules in CHCl<sub>3</sub>.

Compound	$\lambda_{\text{abs}}^{\text{[a]}}$ [nm]	$\log \epsilon$	$\lambda_{\text{em}}$ [nm]	Stokes shift [cm <sup>-1</sup> ]	$\Phi_{\text{F}}^{\text{[b]}}$	$\tau_{\text{F}}$ [ns]	$k_{\text{r}}$ [ $\times 10^8 \text{ s}^{-1}$ ] <sup>[c]</sup>	$k_{\text{nr}}$ [ $\times 10^8 \text{ s}^{-1}$ ] <sup>[d]</sup>
2	655	5.04	672	386	0.81	5.29	1.53	0.36
4	747	5.09	756	159	0.18	2.14	0.84	3.83
5	733	4.88	782	855	0.35	3.34	1.05	1.95
6a	699	5.08	712	261	0.11	0.61	1.80	14.6
8	756	5.04	773	291	0.24	2.31	1.04	3.29
9	803	5.11	847	647	0.14	1.07	1.31	8.04
10	839	4.89	–	–	–	–	–	–
11	638	4.92	654	383	0.75	6.00	1.25	0.42

[a] Only the longest absorption maxima are shown. [b] Absolute fluorescence quantum yields. [c] Rate constant for radiative decay:  $k_{\text{r}} = \Phi_{\text{F}}/\tau_{\text{F}}$ . [d] Rate constant for non-radiative decay:  $k_{\text{nr}} = (1 - \Phi_{\text{F}})/\tau_{\text{F}}$ .

structure of PPAB. The slightly small  $\Phi_{\text{F}}$  value and short fluorescence lifetime ( $\tau_{\text{F}}$ ) of **6a** ( $\Phi_{\text{F}} = 0.11$ ,  $\tau_{\text{F}} = 0.61$  ns) was due to an enhanced non-radiative decay process reflecting the excited-state dynamics of this molecule. Upon elongation of the thienyl substituents to bithienyl from **6a** to **8**, the  $\Phi_{\text{F}}$  and  $\tau_{\text{F}}$  values recovered due to suppression of the flexibility of the substitu-

ents. The  $\Phi_{\text{F}}$  and  $\tau_{\text{F}}$  values then decreased when the substituents were further elongated to terthienyl in the case of **9**.

### Synthesis of PPAB dimer

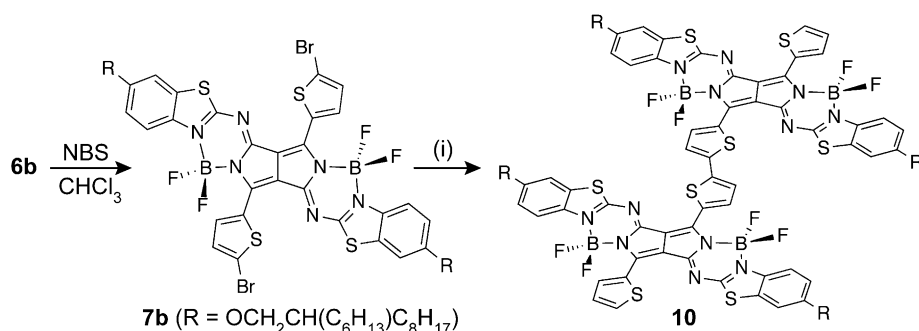
Since the substituents on the pyrrolopyrrole moiety give significant perturbation of the optical properties of PPAB, further enhanced interchromophore interactions could be expected for dimer or oligomer systems of PPAB. The PPAB dimer **10** was successfully synthesized in 3.6% yield from a homo-coupling reaction of **7b** through Pd-catalyzed borylation with bis(pinacolato)diboron (pinB)<sub>2</sub><sup>[19]</sup> and an in situ cross-coupling sequence (Scheme 3).<sup>[18]</sup> Compound **7b** was used instead of **7a** to improve the solubility of the dimer molecule.

The structure of **10** was confirmed by HR-MALDI-FT-ICR-MS, which demonstrated a molecular ion peak at  $m/z = 2280.0281$  ( $[M^+]$ ; calcd for C<sub>120</sub>H<sub>154</sub>B<sub>4</sub>F<sub>8</sub>N<sub>12</sub>O<sub>4</sub>S<sub>8</sub>: 2280.0278). In the <sup>1</sup>H NMR spectrum in CD<sub>2</sub>Cl<sub>2</sub> at room temperature, peaks corresponding to the thienyl substituents and benzothiazole units were observed at  $\delta = 9.32$  (2H), 9.06

(2H), 7.96 (2H), 7.83 (4H), 7.67 (2H), 7.28 (2H), 7.15 (2H), and 7.07 (6H) ppm, reflecting the free-rotation of the bithienyl moiety at this temperature and the chemically identical natures of the monomer units. Surprisingly, compound **10** showed panchromatic absorption across the UV/Vis/NIR regions with four absorption maxima at 374, 580, 680, and 839 nm, which is not a simple redshift as expected from the above mentioned results (Figure 4).

Since only a very small difference in the absorption spectrum was reported in the case of the bithienyl-bridged porphyrin dimer, the contribution from exciton interactions would be negligible in the case of **10**.<sup>[21]</sup> To give an in-depth insight into these significant changes in absorption from monomer to dimer,

DFT and TDDFT calculations were performed on model structures **M-5a** (*s-cis*), **M-5b**, and **M-5c** (*s-trans*) with dihedral angles of 0, 90, and 180°, respectively. In all the cases, the four frontier orbitals, HOMO–1 and HOMO, and LUMO and LUMO + 1, were generated by a linear combination of the HOMO of **M-1** and the LUMO of **M-1**, respectively (Figure 5). Based on the



**Scheme 3.** Synthesis of PPAB dimer **10**. Reagents and conditions: (i) Bis(pinacolate)diboron,  $[\text{PdCl}_2(\text{dppf})]$ , KOAc, DMF, 80 °C, 90 min.

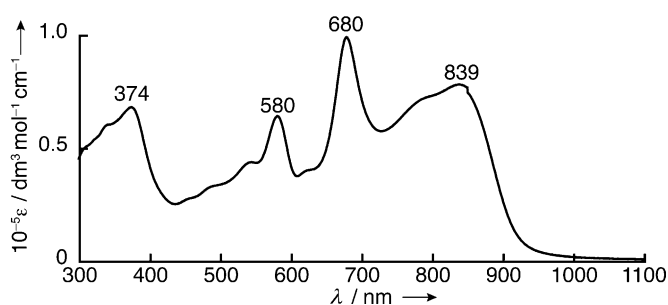


**Figure 4.** UV/Vis/NIR spectrum of PPAB dimer **10** in  $\text{CHCl}_3$ .

TDDFT calculations, the main absorption in the lowest energy region consists of transitions between these orbitals, and the transition energies vary depending on the dihedral angles (Table 3). The theoretical absorption of **M-5b** appears to be similar to that of **M-1**, indicating small interactions between the PPAB moieties in this conformation. In contrast, a bathochromic shift of the main absorption band was predicted for **M-5a** at 872 nm and for **M-5c** at 837 nm compared with that of **M-5b** at 644 nm. These results are indicative of enhanced

interaction between the PPAB moieties due to the effective extension of the conjugation through the bithienyl bridge. Taking into consideration the free-rotational behavior of the bithienyl unit in **10** proposed based on the  $^1\text{H}$  NMR spectrum, the observed absorption spectrum of **10** can be explained in terms of the presence of conformers with different dihedral angles in solution. In contrast to the unique absorption spectrum, compound **10** is non-fluorescent

due to its flexible structure, which may enhance non-radiative decay processes.

### Electrochemistry

To experimentally estimate the HOMO and LUMO energy levels, the redox potentials of PPAB were measured by cyclic voltammetry in *o*-dichlorobenzene containing 0.1 M tetra-*n*-butylammonium perchlorate as a supporting electrolyte (Figure 6). All of the PPAB compounds exhibited one or two reversible oxidations and reductions. The redox potentials as well as the experimental HOMO and LUMO energy levels determined by the first oxidation and reduction potentials (**Ox1** and **Red1**) are summarized in Table 4. Both **Ox1** and **Red1** shifted positively when the heteroaromatic ring moieties became larger from monocyclic pyridine (**1**: 0.43 V and  $-1.33$  V vs.  $\text{Fc}^+/\text{Fc}$ ) to bicyclic benzothiazole and quinoline (**2**: 0.62 V and  $-1.06$  V and **3**: 0.51 V and  $-1.15$  V). The potential difference between **Ox1** and **Red1** ( $\Delta E$ ) of **2** (1.68 V) and **3** (1.66 V) decreased relative to **1** (1.76 V) due to the greater extent of the positive shift of the **Red1** than that of **Ox1**. In contrast,

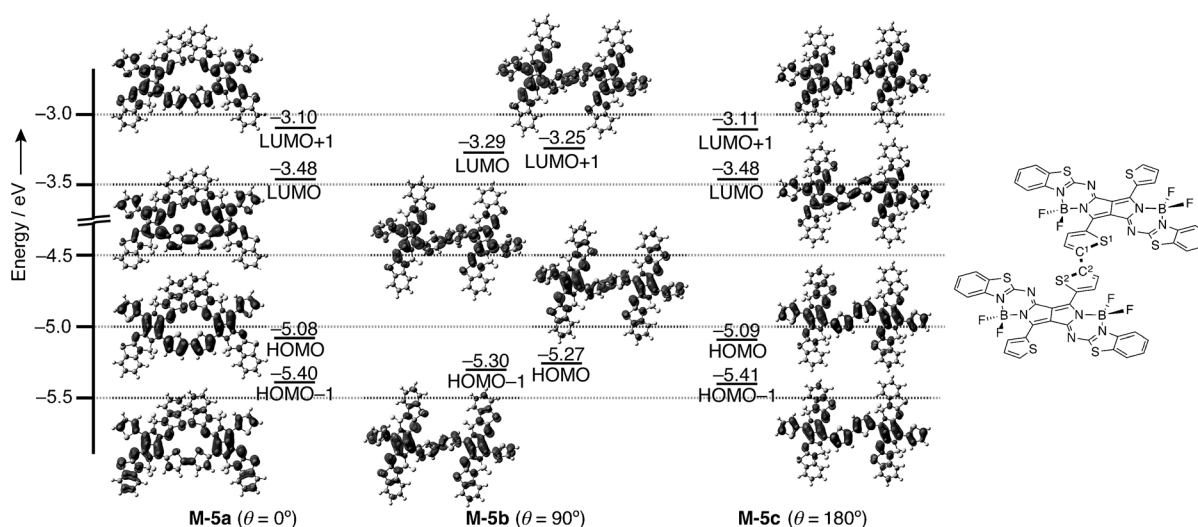


**Figure 5.** Frontier molecular orbitals of PPAB dimer model structures, **M-5a–M-5c** (B3LYP/6-31G(d)).  $\theta$  is defined by the dihedral angle of  $\text{S}^1\text{–C}^1\text{–C}^2\text{–S}^2$ . 2-Hexyldecyloxy substituents were omitted in the model structures for simplicity.

**Table 3.** Summary of TDDFT calculations of PPAB dimer model structures, **M-5a–M-5c** (B3LYP/6-31G(d)).

Compound	$\theta$ [°] <sup>[a]</sup>	Energy [nm]	$f^{[b]}$	Wavefunction <sup>[c]</sup>
<b>M-5a</b>	0	872	0.45	+0.709 L←H>+...
		628	0.95	+0.561 L+1←H>-0.433 L←H-1>+...
		553	0.53	+0.667 L←H-2>+0.190 L+1←H-1>+...
		483	0.42	+0.686 L←H-4>+...
		459	0.18	+0.678 L+2←H>+...
<b>M-5b</b>	90	644	1.11	+0.585 L+1←H-1>-0.403 L←H>+...
		631	0.16	+0.523 L+1←H>-0.479 L←H-1>+...
		473	0.21	+0.500 L←H-3>+0.410 L+1←H-2> -0.209 L←H-3>-0.110 L+1←H-4>+...
		453	0.87	+0.499 L←H-5>+0.413 L+1←H-4> +0.201 L←H-5>+0.147 L+1←H-2>+...
<b>M-5c</b>	180	837	1.12	+0.709 L←H>+...
		641	0.16	+0.565 L+1←H>-0.429 L←H-1>+...
		592	0.36	+0.675 L+1←H-1>+0.201 L←H-2>+...
		554	0.55	+0.666 L←H-2>-0.195 L+1←H-1>+...
		478	0.39	+0.675 L←H-4>-0.129 L+1←H-3>+...
		455	0.17	+0.675 L+2←H>-0.106 L←H-4>+...

[a] Dihedral angle of S<sup>1</sup>-C<sup>1</sup>-C<sup>2</sup>-S<sup>2</sup> in Figure 5. [b] Oscillator strength. [c] The wavefunctions are based on the eigenvectors predicted by TDDFT. H and L represent the HOMO and LUMO, respectively.

creasing the number of thiophene units. These results and variation of the  $\Delta E$  values are in good agreement with the redshift of the absorption of these PPAB molecules and broadly reproduced by the theoretical calculations (Figure 1).

Cyclic voltammetry measurements were also performed on the dimer **10**, demonstrating **Ox1** at 0.36 V and **Red1** at -0.95 V. This result is very comparable to that of **8** with bithienyl substituents, indicating that the redox processes may occur independently on each PPAB moiety.

### Potential application of PPAB in bulk heterojunction photovoltaic cells

Because of the intense absorption in the Vis/NIR regions and the highly conjugated planar structures, PPAB are potential candidates for bulk heterojunction organic photovoltaics (BHJ-OPV). Based on the HOMO and LUMO energy levels estimated experimentally by cyclic voltammetry (Table 4), possible p-type PPAB molecules with an appropriate LUMO

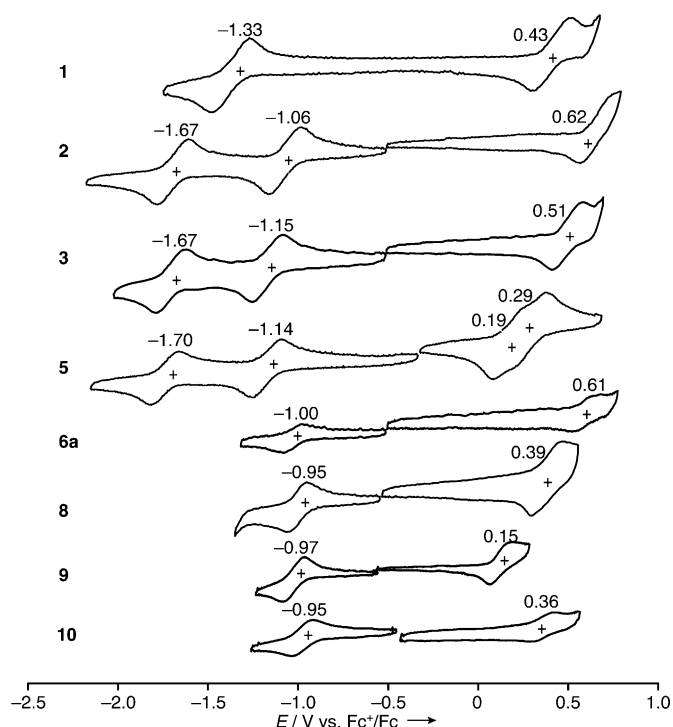


**Figure 6.** Cyclic voltammograms of PPAB molecules (0.5 mM) in *o*-dichlorobenzene containing 0.1 M tetra-*n*-butylammonium perchlorate as a supporting electrolyte at a scan rate of 100 mV s<sup>-1</sup>. Values are half-wave potentials.

changing the substituents on the pyrrolopyrrole moiety caused a negative shift of **Ox1**. Compound **5** with *p*-piperidinophenyl substituents exhibited **Ox1** at 0.19 V, which is significantly shifted to the negative with respect to **2**, whereas a gradual negative shift of **Ox1** was observed in the order from **6a** (0.61 V) to **8** (0.39 V) and further to **9** (0.15 V) upon in-

**Table 4.** Summary of electrochemical properties of PPAB molecules<sup>[a]</sup> and experimental HOMO and LUMO energy levels ( $E_{\text{HOMO}}$  and  $E_{\text{LUMO}}$ ).

Compound	$E^{1/2}_{\text{ox}}$ <sup>[b]</sup> [V]	$E^{1/2}_{\text{red}}$ <sup>[b]</sup> [V]	$\Delta E$ <sup>[c]</sup> [V]	$E_{\text{HOMO}}$ <sup>[d]</sup> [eV]	$E_{\text{LUMO}}$ <sup>[e]</sup> [eV]
<b>1</b>	0.43	-1.33	1.76	-5.22	-3.47
<b>2</b>	0.62	-1.06, -1.67	1.68	-5.42	-3.74
<b>3</b>	0.51	-1.15, -1.67	1.66	-5.31	-3.65
<b>5</b>	0.19, 0.29	-1.14, -1.70	1.33	-4.99	-3.66
<b>6a</b>	0.61	-1.00	1.61	-5.41	-3.80
<b>8</b>	0.39	-0.95	1.34	-5.19	-3.83
<b>9</b>	0.15	-0.97	1.12	-4.95	-3.80
<b>10</b>	0.36	-0.95	1.31	-5.16	-3.85

[a] Electrochemical measurements on **4** could not be performed due to the low yield of **4**. [b] Determined by cyclic voltammetry (conditions: 0.5 mM *o*-DCB solutions of analyte containing 0.1 M tetrabutylammonium perchlorate as a supporting electrolyte at a scan rate of 100 mV s<sup>-1</sup>). Potentials are given relative to the ferrocenium/ferrocene couple. [c]  $\Delta E$ : difference between the **Ox1** and **Red1**. [d]  $E_{\text{HOMO}} = -(\text{Ox1} + 4.8)$  eV. [e]  $E_{\text{LUMO}} = -(\text{Red1} + 4.8)$  eV.

energy level for n-type phenyl-C<sub>61</sub>-butyric acid methyl ester (PC<sub>61</sub>BM) were examined. Since slightly higher LUMO energy levels of donor molecules by 0.2–0.3 eV relative to those of acceptor molecules are necessary for efficient charge separation, compound **1** with its LUMO at -3.47 eV has high potential within this series of PPAB molecules. All of the other PPAB molecules including the dimer **10** possess a low-lying LUMO at -3.65–-3.85 eV, which is fairly close to the LUMO energy level of PC<sub>61</sub>BM at -3.8 eV. Further necessary information before device fabrication, such as a p/n blend ratio, can be deduced based on time-resolved microwave conductivity (TRMC) measurements<sup>[21–23]</sup> using monochromatic light pulse from a nanosecond laser (laser-flash)<sup>[24–27]</sup> or white-light pulse from a Xe flash-lamp (Xe-flash)<sup>[11]</sup> as photoexcitation sources. The laser-

flash-TRMC measurements demonstrated that the maximum transient conductivity,  $\varphi \Sigma \mu_{\max}$  in which  $\varphi$  and  $\Sigma \mu$  represent charge carrier generation efficiency and the sum of hole and electron mobilities, respectively, was significantly enhanced for **1** upon blending with PC<sub>61</sub>BM (= 1:1 in weight fraction (w/w)) compared with those of the other PPAB molecules **2**, **6a**, and **8** (Figure 7a). This result also supports the potential utility of

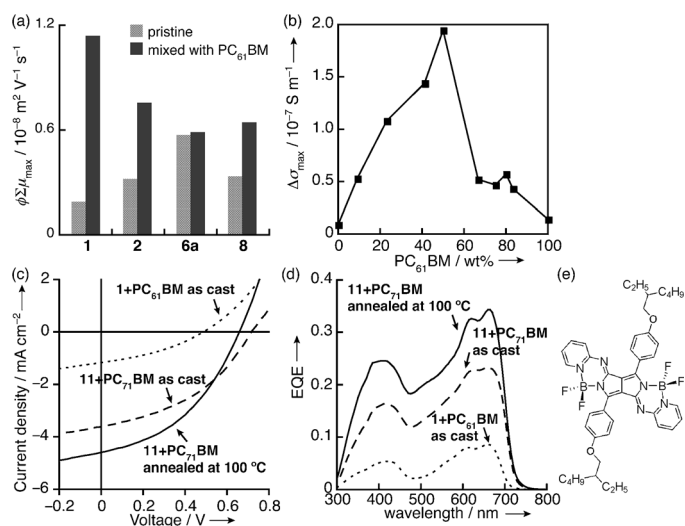


**Figure 7.** (a) Maximum TRMC signals ( $\varphi \Sigma \mu_{\max}$ ) of pristine PPAB molecule and PPAB/PC<sub>61</sub>BM (1:1 (w/w)) drop-cast films from chloroform solutions measured by laser-flash TRMC (ex. 355 nm); (b)  $\Delta \sigma_{\max}$  of Xe-flash TRMC of drop-cast films of 1:PC<sub>61</sub>BM plotted as a function of PC<sub>61</sub>BM content. 100wt% PC<sub>61</sub>BM represents pure PC<sub>61</sub>BM; (c)  $J/V$  curves of the PPAB/PC<sub>61(71)</sub>BM (1:1 (w/w)) (..... = 1/PC<sub>61</sub>BM, spin-coated from a chloroform solution containing 0.7 v/v% DIO, without thermal annealing; --- = 11/PC<sub>71</sub>BM, spin-coated from a chloroform solution containing 0.5 v/v% DIO, without thermal annealing; solid line: 11:PC<sub>71</sub>BM, spin-coated from a chloroform solution containing 0.5 v/v% DIO, with 100 °C annealing); (d) EQE spectra of the devices of (c); (e) Structure of **11**.

**1** as a p-type material in BHJ-OPV using PC<sub>61</sub>BM as an acceptor. Following this, Xe-flash TRMC measurements on blend films of **1** and PC<sub>61</sub>BM were performed to optimize the p/n blend ratio. The Xe-flash TRMC provided photoconductivity maxima ( $\Delta \sigma_{\max}$ ), which includes information about not only the yield and local mobility of charge carriers, but also their lifetime because of the lower photoirradiation density and time resolution than those of laser-flash TRMC. From the maximum of the  $\Delta \sigma_{\max}$  located at 50 wt% of PC<sub>61</sub>BM, the optimized blend ratio was determined as 1:1 (w/w) of **1** and PC<sub>61</sub>BM (Figure 7b). A BHJ-OPV device with a Glass/ITO/ZnO/BHJ/MoO<sub>3</sub>/Ag inverted cell structure was fabricated using an active layer spin-coated from a chloroform solution of this ratio of **1** and PC<sub>61</sub>BM containing 0.5 volume% of solvent additive 1,8-diiodooctane (DIO). This device gave a power conversion efficiency (PCE) of 0.20% with an open-circuit voltage ( $V_{oc}$ ) of 0.49 V, a short-circuit current density ( $J_{sc}$ ) of 1.16 mA cm<sup>-2</sup>, and a fill factor ( $FF$ ) of 0.35 under AM1.5G illumination (100 mW cm<sup>-2</sup>; Figure 7c,d and Table 5). The low performance was explained by roughness of the active layer due to aggregation of **1**, which was ob-

Blend	Solvent	$L^{[a]}$ [nm]	Anneal	$J_{sc}$ [mA cm <sup>-2</sup> ]	$V_{oc}$ [V]	$FF$	PCE [%]
1:PC <sub>61</sub> BM	CF <sup>[b]</sup> 0.7% v/v	DIO 140		1.16	0.49	0.35	0.20
11:PC <sub>71</sub> BM	CF <sup>[b]</sup> 0.5% v/v	DIO 200		3.62	0.72	0.41	1.07
11:PC <sub>71</sub> BM	CF <sup>[b]</sup> 0.5% v/v	DIO 200	100 °C	4.60	0.66	0.42	1.27

The inverted cell structure (ITO/ZnO/BHJ/MoO<sub>3</sub>/Ag) was employed.  
[a] Active layer thickness. [b] CF represents chloroform.

served by optical microscopy and surface-topography of AFM (see the Supporting Information, Figures S1 and S2).

To improve the solubility of **1**, compound **11** bearing 2-ethylhexyloxy substituents instead of the octyloxy substituents was synthesized (Figure 7e). A similar device structure with an as-cast active layer of **11** and phenyl-C<sub>71</sub>-butyric acid methyl ester (PC<sub>71</sub>BM) (= 1:1 (w/w)), which was used instead of PC<sub>61</sub>BM to improve the photoabsorption in the visible region,<sup>[28]</sup> exhibited a better PCE of 1.07% after optimization of the device fabrication conditions, such as the spin-coat temperature, the amount of additive DIO, and the thickness of the active layer. Further improvement in PCE up to 1.27% with  $V_{oc}$  of 0.66 V,  $J_{sc}$  of 4.60 mA cm<sup>-2</sup>, and  $FF$  of 0.42 was achieved by annealing the BHJ layer at 100 °C (Figure 7c,d and Table 5). AFM measurements on this annealed BHJ layer demonstrated improvement in the surface roughness, indicating the formation of a BHJ structure having nanometer dimension (see the Supporting Information, Figure S2).

## Conclusion

The TiCl<sub>4</sub>-mediated Schiff-base formation reaction of DPP opened access to a series of PPAB molecules containing a variety of heteroaromatic ring moieties and substituents on the pyrrolopyrrole moiety, which were designed based on theoretical calculations with the aim of shifting the main intense absorption and fluorescence to the red. The fluorescence quantum yields of these PPAB molecules were comparatively high relative to other conventional fluorophores in the corresponding regions. The results of this study indicate that the introduction of electron-donating substituents to the pyrrolopyrrole moiety, as exemplified by oligothieryl substituted PPAB molecules **6a**, **8**, and **9**, appears to be a very practical strategy towards NIR absorption and fluorescence emission. Extension of the conjugated systems was further achieved in the dimeric system, which unexpectedly exhibited panchromatic absorption in the UV/Vis/NIR regions due to the presence of conformers with various dihedral angles. With this series of PPAB molecules in hand, their application in BHJ-OPV devices was investigated. Based on electrochemical and TRMC screening, compound **1** was selected as a potential candidate for this purpose. By optimizing several conditions including the solubility of the PPAB, the choice of fullerene derivatives as an acceptor, and the device fabrication conditions, a PCE of 1.27% with  $V_{oc}$  of 0.66 V,  $J_{sc}$  of 4.60 mA cm<sup>-2</sup>, and  $FF$  of 0.42 was achieved using a blend film of **11** and PC<sub>71</sub>BM (= 1:1 (w/w)) as an active layer.

Further improvement of the OPV performance can be expected, if the photoabsorption of PPAB in the higher energy visible region can be enhanced. In this respect, the dimer **10** should be highly promising. However, most of the PPAB molecules synthesized to date are not appropriate due to their low-lying LUMO energy levels, which originate from the PPAB structures consisting of benzothiazole heteroaromatic ring moieties. Since PPAB with pyridine rings has a suitable LUMO energy level for PC<sub>61(71)</sub>BM, control of the photoabsorption based on this PPAB structure by changing the substituents on the pyrrolopyrrole moiety or by homo-oligomerization will be the next topic to be pursued with the aim of achieving a high PCE in the PPAB-based BHJ-OPV. Furthermore, from a synthetic point of view, the TiCl<sub>4</sub>-mediated Schiff-base formation reaction is a versatile synthetic method to convert other conjugated bicyclic lactam molecules to dimeric *aza*-BODIPY analogues. Research along both of these directions is currently being undertaken and will be reported in due course.

## Experimental Section

### General procedures

Electronic absorption spectra were recorded on a JASCO V-570 spectrophotometer. Fluorescence spectra were measured on a Hitachi F-4500 spectrofluorimeter or on a Horiba Fluorolog-3 spectrofluorimeter. Absolute fluorescence quantum yields were measured on a Hamamatsu Photonics C9920-03G calibrated integrating sphere system. The fluorescence lifetime was measured with a picosecond light pulser (Hamamatsu Photonics C4725: 408 nm, 59 ps FWHM) and a streak-scope (Hamamatsu Photonics C4334-02). <sup>1</sup>H NMR spectra were recorded on a Bruker AVANCE III 500 spectrometer (operating at 500.133 MHz for <sup>1</sup>H) using residual solvent as an internal reference for <sup>1</sup>H ( $\delta$  = 7.26 ppm for CDCl<sub>3</sub> and  $\delta$  = 5.32 ppm for CD<sub>2</sub>Cl<sub>2</sub>). High-resolution mass spectra were recorded on a Bruker Daltonics solarix 9.4T spectrometer. Cyclic voltammograms were recorded on a Hokuto Denko HZ5000 potentiostat under a nitrogen atmosphere in *o*-dichlorobenzene solutions with 0.1 M tetra-*n*-butylammonium perchlorate as a supporting electrolyte. Measurements were made with a glassy carbon electrode (area = 0.07 cm<sup>2</sup>), an Ag/AgCl reference electrode, and a Pt-wire counter electrode. The concentration of the solution was fixed at 0.5 mM and the sweep rates were set to 100 mV s<sup>-1</sup>. The ferrocenium/ferrocene (Fc<sup>+</sup>/Fc) couple was used as an internal standard. Preparative separations were performed by using alumina and silica gel column chromatography (Wako) and recycling preparative GPC-HPLC (JAI LC-9201 with preparative JAIGEL-2H and -2.5H columns using chloroform as an eluent). Thin-layer chromatography (TLC) was performed with aluminum sheet silica gel 60 F<sub>254</sub> (Merck). Toluene, which was used for the synthesis of PPAB, was distilled over CaH<sub>2</sub> prior to use. All the other reagents and solvents were of commercial reagent grade and were used without further purification except where noted.

### Crystallographic data collection and structure refinement

Suitable crystals of **6b** for X-ray analysis were obtained from slow diffusion of hexane into a toluene solution. Data collection for **6b** was carried out at -173(2) °C on a Bruker APEXII CCD diffractometer with MoK $\alpha$  radiation ( $\lambda$  = 0.71073 Å). The structures were solved by a direct method (SHLEXS-97)<sup>[29]</sup> and refined using a full-matrix

least squares technique (SHELXL-2013).<sup>[29]</sup> Yadokari-XG software was used as a GUI for SHELXL-2013.<sup>[30]</sup> CCDC-1021750 contains the supplementary crystallographic data for **6b**. This data can be obtained free of charge from The Cambridge Crystallographic Data Centre via [www.ccdc.cam.ac.uk/data\\_request/cif](http://www.ccdc.cam.ac.uk/data_request/cif).

### Computational methods

The Gaussian 09 software package<sup>[31]</sup> was used to carry out DFT and TDDFT calculations using the B3LYP functional with 6-31G(d) basis set. Structural optimization was performed on **M-1-4** as model compounds of **2**, **4**, **5**, and **6a**, respectively.

### Time-resolved microwave conductivity

A resonance cavity was used to obtain a high degree of sensitivity in the conductivity measurement. The resonance frequency and microwave power were set at about 9.1 GHz and 3 mW, respectively, so that the electric field of the microwave was sufficiently small not to disturb the motion of charge carriers. Nanosecond laser pulse at third-harmonic generation (THG; 355 nm) of a Nd:YAG laser (Continuum, Surelite II, 5–8 ns pulse duration, 10 Hz) or microsecond white-light pulse from a Xe flash lamp was used as an excitation source. The photoconductivity  $\Delta\sigma$  was obtained by  $\Delta P_r / (AP_r)$ , in which  $\Delta P_r$ ,  $A$ , and  $P_r$  are the transient power change of reflected microwave from a cavity, the sensitivity factor, and the reflected microwave power, respectively. The power of the white-light pulse was 0.3 mJ cm<sup>-2</sup> pulse<sup>-1</sup>. The samples were drop-cast onto a quartz plate from solutions of PPAB and PC<sub>61(71)</sub>BM and dried in a vacuum oven. The TRMC experiments were performed under ambient conditions at room temperature.

### Organic photovoltaic cell

A ZnO layer was fabricated onto a cleaned ITO layer by spin-coating of ZnO precursor solution (0.1 g mL<sup>-1</sup> zinc acetate dihydrate and 0.028 g mL<sup>-1</sup> ethanolamine in 2-methoxyethanol). The substrate was annealed on a hot plate at 200 °C for 30 min. An active layer consisting of the PPAB and PC<sub>61(71)</sub>BM (purchased from Frontier Carbon Inc.) was cast on top of the ZnO layer in a nitrogen glovebox by spin-coating. The thickness was controlled by changing the rotation speed and was measured by a surface profiler, an ULVAC model Dektak 150. An anode consisting of 10 nm MoO<sub>3</sub> and 100 nm Ag layers was sequentially deposited through a shadow mask on top of the active layers by thermal evaporation in a vacuum chamber. The resulting device configuration was ITO (120–160 nm)/ZnO (30 nm)/active layer (140–200 nm)/MoO<sub>3</sub> (10 nm)/Ag (100 nm) with an active area of 7.1 mm<sup>2</sup>. Current–voltage ( $J/V$ ) curves were measured using a source-measure unit (ADCMT Corp., 6241 A) under AM1.5G solar illumination at 100 mW cm<sup>-2</sup> (1 sun, monitored by a calibrated standard cell, Bunko Keiki SM-250 KD) from a 300 W solar simulator (SAN-EI Corp., XES-301S). EQE spectra were measured using a Bunko Keiki model BS-520BK equipped with a Keithley model 2401 source meter. The monochromated light power was calibrated with a silicon photovoltaic cell, Bunko Keiki model S1337-1010BQ.

### Synthesis of PPAB

**Synthesis of 4:** To a toluene solution (7 mL) of **DPP-1** (96 mg, 0.18 mmol) and **HA-1** (301 mg, 1.78 mmol) heated at reflux were added TiCl<sub>4</sub> (0.25 mL, 2.3 mmol) and triethylamine (1.0 mL, 7.2 mmol). After consumption of **DPP-1**, which was confirmed by TLC analysis, BF<sub>3</sub>·OEt<sub>2</sub> (1.0 mL, 8.1 mmol) was added, and resulting

solution was heated at reflux for 4 h. The reaction mixture was poured into 300 mL of water, and the organic phase was extracted with  $\text{CHCl}_3$ . The organic layer was dried over sodium sulfate, and the solvent was removed. The crude product was purified by silica gel column chromatography using  $\text{CHCl}_3$  as an eluent. Recrystallization from chloroform and methanol provided **4** as a brown powder (1.7 mg, 1.0%).  $^1\text{H NMR}$  (500 MHz,  $\text{CDCl}_3$ ):  $\delta$  = 8.73 (d, 4H,  $J$  = 8.5 Hz), 8.26 (d, 2H,  $J$  = 7.0 Hz), 8.17 (d, 2H,  $J$  = 8.0 Hz), 7.82 (dd, 2H,  $J_1 = J_2 = 7.6$  Hz), 7.77 (d, 2H,  $J$  = 7.6 Hz), 7.74 (d, 2H,  $J$  = 6.8 Hz), 7.62 (dd, 2H,  $J_1 = J_2 = 7.7$  Hz), 7.17 (d, 4H, 8.6 Hz), 4.18 (t, 4H,  $J$  = 6.5 Hz), 1.91–1.25 (m, 24H), 0.92 ppm (t, 6H,  $J$  = 6.5 Hz); UV/Vis ( $\text{CHCl}_3$ ):  $\lambda_{\text{max}}$  ( $\epsilon$ ) = 355 (13 000), 440 (23 000), 497 (16 000), 684 (33 000), 747 nm ( $120\,000\text{ mol}^{-1}\text{ dm}^3\text{ cm}^{-1}$ ); HR-MALDI-FT-ICR-MS:  $m/z$  calcd for  $\text{C}_{56}\text{H}_{54}\text{B}_2\text{F}_4\text{N}_6\text{O}_2$ : 990.4425 [ $M^+$ ]; found: 990.4428.

**Synthesis of 5:** Compound **5** was synthesized under similar reaction conditions to **4** from **DPP-2** (102 mg, 0.22 mmol), **HA-2** (330 g, 2.2 mmol),  $\text{TiCl}_4$  (0.30 mL, 2.7 mmol), triethylamine (1.0 mL, 7.2 mmol), and  $\text{BF}_3\cdot\text{OEt}_2$  (0.75 mL, 6.1 mmol). The reaction mixture was purified similarly to **4**, to give **5** as a violet powder (10.4 mg, 5.8%).  $^1\text{H NMR}$  (500 MHz,  $\text{CDCl}_3$ ):  $\delta$  = 8.54 (broad, 4H), 7.91 (d,  $J$  = 8.2 Hz, 2H), 7.72 (d,  $J$  = 8.0 Hz, 2H), 7.50 (dd,  $J_1 = J_2 = 8.0$  Hz, 2H), 7.38 (dd,  $J_1 = J_2 = 7.7$  Hz, 2H), 7.31 (broad, 4H), 3.58 (broad, 8H), 1.91 (broad, 8H), 1.77 ppm (broad, 4H); UV/Vis ( $\text{CHCl}_3$ ):  $\lambda_{\text{max}}$  ( $\epsilon$ ) = 329 (27 000), 354 (29 000), 516 (44 000), 733 nm ( $75\,000\text{ mol}^{-1}\text{ dm}^3\text{ cm}^{-1}$ ); HR-MALDI-FT-ICR-MS:  $m/z$  calcd for  $\text{C}_{42}\text{H}_{36}\text{B}_2\text{F}_4\text{N}_8\text{S}_2$ : 814.2622 [ $M^+$ ]; found: 814.2622.

**Synthesis of 6a:** Compound **6a** was synthesized under similar reaction conditions to **4** from **DPP-3** (199 mg, 0.66 mmol), **HA-3a** (1.0 g, 3.6 mmol, for the synthesis of **HA-3a**, see the Supporting Information),  $\text{TiCl}_4$  (0.50 mL, 4.6 mmol), triethylamine (2.5 mL, 18 mmol), and  $\text{BF}_3\cdot\text{OEt}_2$  (2.0 mL, 16 mmol). The reaction mixture was purified similarly to **4**, to give **6a** as a green powder (235 mg, 39%).  $^1\text{H NMR}$  (500 MHz,  $\text{CDCl}_3$ ):  $\delta$  = 9.07 (d,  $J$  = 4.0 Hz, 2H), 7.95 (d,  $J$  = 9.1 Hz, 2H), 7.85 (d, 2H), 7.33 (dd,  $J_1 = 4.0$  Hz,  $J_2 = 5.0$  Hz, 2H), 7.18 (s, 2H), 7.10 (d,  $J$  = 9.1 Hz, 2H), 4.02 (t,  $J$  = 6.5 Hz, 4H), 1.82 (m, 4H), 1.49–1.30 (m, 20H), 0.89 ppm (t,  $J$  = 6.9 Hz, 6H);  $\lambda_{\text{max}}$  ( $\epsilon$ ) = 348 (35 000), 462 (20 000), 638 (43 000), 699 nm ( $120\,000\text{ mol}^{-1}\text{ dm}^3\text{ cm}^{-1}$ ); HR-MALDI-FT-ICR-MS:  $m/z$  calcd for  $\text{C}_{44}\text{H}_{46}\text{B}_2\text{F}_4\text{N}_6\text{O}_2\text{S}_4$ : 916.2683 [ $M^+$ ]; found: 916.2683.

**Synthesis of 6b:** Compound **6b** was synthesized under similar reaction conditions to **4** from **DPP-3** (113 mg, 0.38 mmol), **HA-3b** (742 mg, 1.9 mmol for the synthesis of **HA-3b**, see the Supporting Information),  $\text{TiCl}_4$  (0.25 mL, 2.3 mmol), triethylamine (1.0 mL, 7.2 mmol), and  $\text{BF}_3\cdot\text{OEt}_2$  (1.0 mL, 8.1 mmol). The reaction mixture was purified similarly to **4**, to give **6b** as a green powder (128 mg, 30%).  $^1\text{H NMR}$  (500 MHz,  $\text{CDCl}_3$ ):  $\delta$  = 9.07 (d,  $J$  = 3.9 Hz, 2H), 7.95 (d,  $J$  = 9.1 Hz, 2H), 7.85 (d,  $J$  = 5.0 Hz, 2H), 7.33 (dd,  $J_1 = J_2 = 4.2$  Hz, 2H), 7.19 (s, 2H), 7.11 (d,  $J$  = 9.1 Hz, 2H), 3.90 (d,  $J$  = 5.6 Hz, 4H), 1.81–1.29 (m, 50H), 0.90–0.87 ppm (m, 12H); HR-MALDI-FT-ICR-MS:  $m/z$  calcd for  $\text{C}_{60}\text{H}_{78}\text{B}_2\text{F}_4\text{N}_6\text{O}_2\text{S}_4$ : 1140.5187 [ $M^+$ ]; found: 1140.5187;

**Synthesis of 7a:** *N*-bromosuccinimide (51.6 mg, 0.29 mmol) was added slowly to a  $\text{CHCl}_3$  solution (15 mL) of **5a** (130 mg, 0.14 mmol), and the resulting solution was stirred for three days. The mixture was then poured into an aqueous solution of sodium thiosulfate, and the organic phase was extracted with  $\text{CHCl}_3$ . The organic layer was dried over sodium sulfate, and the solvent was removed. Recrystallization from  $\text{CHCl}_3$  and methanol provided **7a** as a green powder (138 mg, 92%).  $^1\text{H NMR}$  (500 MHz,  $\text{CDCl}_3$ ):  $\delta$  = 8.94 (d,  $J$  = 4.3 Hz, 2H), 7.95 (d,  $J$  = 9.2 Hz, 2H), 7.29 (d,  $J$  = 4.3 Hz, 2H), 7.18 (s, 2H), 7.12 (d,  $J$  = 9.1 Hz, 2H), 4.02 (t,  $J$  = 6.5 Hz, 4H), 1.83 (m, 4H), 1.52–1.30 (m, 20H), 0.90 ppm (t,  $J$  = 7.0 Hz, 6H);  $\lambda_{\text{max}}$  ( $\epsilon$ ) = 355 (42 000), 475 (28 000), 650 (48 000), 713 nm

( $130\,000\text{ mol}^{-1}\text{ dm}^3\text{ cm}^{-1}$ ); HR-MALDI-FT-ICR-MS:  $m/z$  calcd for  $\text{C}_{44}\text{H}_{44}\text{B}_2\text{Br}_2\text{F}_4\text{N}_6\text{O}_2\text{S}_4$ : 1074.0871 [ $M^+$ ]; found: 1074.0871.

**Synthesis of 7b:** Compound **7b** was similarly synthesized and purified to the case of **7a**. Compound **7b** was obtained as a green powder in 93% yield (133 mg).  $^1\text{H NMR}$  (500 MHz,  $\text{CDCl}_3$ ):  $\delta$  = 8.94 (d,  $J$  = 4.3 Hz, 2H), 7.95 (d,  $J$  = 8.9 Hz, 2H), 7.25 (d,  $J$  = 4.3 Hz, 2H), 7.17 (s, 2H), 7.11 (d,  $J$  = 9.1 Hz, 2H), 3.90 (d,  $J$  = 5.7 Hz, 4H), 1.83–1.30 (m, 50H), 0.91–0.87 ppm (m, 12H). HR-MALDI-FT-ICR-MS:  $m/z$  calcd for  $\text{C}_{60}\text{H}_{76}\text{B}_2\text{Br}_2\text{F}_4\text{N}_6\text{O}_2\text{S}_4$ : 1298.3375 [ $M^+$ ]; found: 1298.3375.

**Synthesis of 8:** Compound **7a** (24 mg, 0.022 mmol) and thiophene-2-boronic acid (14 mg, 0.11 mmol) were dissolved in toluene (0.6 mL), and a small amount of Aliquat 336 and 2.0 M aqueous solution of  $\text{Na}_2\text{CO}_3$  (0.4 mL) was added. After degassing under nitrogen bubbling for 30 min, tetrakis(triphenylphosphine)palladium (5.0 mg, 4.3  $\mu\text{mol}$ ) was added, and the resulting solution was heated at reflux for 1 hour. After cooling to room temperature, the resulting mixture was poured into methanol (20 mL), and the precipitate was collected by filtration. Purification of the filtrate by silica gel chromatography using  $\text{CHCl}_3$  as an eluent and recrystallization from  $\text{CHCl}_3$  and methanol provided **8** as a pink powder (11 mg, 45%).  $^1\text{H NMR}$  (500 MHz,  $\text{CDCl}_3$ ):  $\delta$  = 9.18 (d,  $J$  = 4.2 Hz, 2H), 7.99 (d,  $J$  = 8.8 Hz, 2H), 7.49 (d,  $J$  = 3.6 Hz, 2H), 7.41 (d,  $J$  = 4.2 Hz, 2H), 7.39 (d,  $J$  = 5.1 Hz, 2H), 7.18 (s, 2H), 7.12–7.10 (m, 4H), 4.03 (t,  $J$  = 6.5 Hz, 4H), 1.83 (m, 4H), 1.51–0.89 (m, 20H), 0.90 ppm (t,  $J$  = 6.9 Hz, 6H);  $\lambda_{\text{max}}$  ( $\epsilon$ ) = 324 (30 000), 389 (36 000), 520 (28 000), 551 (28 000), 687 (40 000), 756 nm ( $110\,000\text{ mol}^{-1}\text{ dm}^3\text{ cm}^{-1}$ ); HR-MALDI-FT-ICR-MS:  $m/z$  calcd for  $\text{C}_{52}\text{H}_{50}\text{B}_2\text{F}_4\text{N}_6\text{O}_2\text{S}_6$ : 1080.2438 [ $M^+$ ]; found: 1080.2437.

**Synthesis of 9:** Compound **7a** (19 mg, 0.018 mmol), 5'-hexyl-2,2'-bithiophene-5-boronic acid pinacol ester (32 mg, 0.085 mmol), [1,1'-bis(diphenylphosphino)ferrocene]palladium(II) dichloride dichloromethane adduct ([ $\text{PdCl}_2(\text{dppf})$ ], 8.1 mg, 9.9  $\mu\text{mol}$ ), and potassium acetate (23 mg, 0.23 mmol) were dissolved in dry DMF (0.6 mL), and the resulting solution was stirred at 80 °C for 15 min. After cooling to room temperature, the resulting mixture was poured into water, and the precipitate was collected by filtration. Purification of the filtrate by silica gel chromatography using  $\text{CHCl}_3$  as an eluent and GPC-HPLC and recrystallization from  $\text{CHCl}_3$  and methanol provided **9** as a dark-blue powder (6.3 mg, 25%).  $^1\text{H NMR}$  (500 MHz,  $\text{CD}_2\text{Cl}_2$ ):  $\delta$  = 9.24 (d,  $J$  = 4.2 Hz, 2H), 7.90 (d,  $J$  = 9.2 Hz, 2H), 7.35 (d,  $J$  = 3.7 Hz, 2H), 7.31 (d,  $J$  = 3.9 Hz, 2H), 7.15 (s, 2H), 7.11–7.09 (m, 6H), 6.76 (d,  $J$  = 3.6 Hz, 2H), 4.00 (t,  $J$  = 6.5 Hz, 4H), 2.84 (t,  $J$  = 7.7 Hz, 4H), 1.82–1.27 (m, 40H), 0.93–0.90 ppm (m, 12H);  $\lambda_{\text{max}}$  ( $\epsilon$ ) = 364 (49 000), 424 (37 000), 583 (37 000), 728 (46 000), 803 nm ( $130\,000\text{ mol}^{-1}\text{ dm}^3\text{ cm}^{-1}$ ); HR-MALDI-FT-ICR-MS:  $m/z$  calcd for  $\text{C}_{72}\text{H}_{78}\text{B}_2\text{F}_4\text{N}_6\text{O}_2\text{S}_8$ : 1412.4070 [ $M^+$ ]; found: 1412.4070.

**Synthesis of 10:** Compound **7b** (88 mg, 0.068 mmol), bis(pinacolate)diboron (0.24 g, 0.94 mmol), potassium acetate (0.15 g, 1.5 mmol) and a catalytic amount of [ $\text{PdCl}_2(\text{dppf})$ ] were dissolved in dry DMF (5 mL), and the resulting solution was stirred at 80 °C for 90 min. After cooling to room temperature, the resulting mixture was poured into methanol, and the precipitate was collected by filtration. Purification of the filtrate by silica gel chromatography using  $\text{CHCl}_3$  as an eluent and GPC-HPLC, and recrystallization from  $\text{CHCl}_3$  and methanol provided **10** as a violet powder (2.8 mg, 3.6%).  $^1\text{H NMR}$  (500 MHz,  $\text{CDCl}_3$ ):  $\delta$  = 9.29 (d,  $J$  = 4.0 Hz, 2H), 9.08 (d,  $J$  = 3.3 Hz, 2H), 8.00 (d,  $J$  = 8.7 Hz, 2H), 7.90 (d,  $J$  = 8.3 Hz, 2H), 7.79 (d,  $J$  = 4.8 Hz, 2H), 7.66 (d,  $J$  = 4.1 Hz, 2H), 7.11 (s, 2H), 7.05 (m, 6H), 3.65 (m, 8H), 1.83–1.20 (m, 100H), 0.90 (m, 24H); (500 MHz,  $\text{CD}_2\text{Cl}_2$ ):  $\delta$  = 9.32 (brs, 2H), 9.06 (brs, 2H), 7.96 (d,  $J$  = 6.0 Hz, 2H), 7.83 (m, 4H), 7.67 (brs, 2H), 7.28 (brs, 2H), 7.15 (brs, 2H), 7.07 (brs, 6H), 3.87 (m, 8H), 1.83–1.20 (m, 100H), 0.90 ppm (m, 24H); UV/Vis ( $\text{CHCl}_3$ ):  $\lambda_{\text{max}}$  ( $\epsilon$ ) = 374 (68 000), 581 (64 000), 679 (99 000),

839 nm ( $78\,000\text{ mol}^{-1}\text{ dm}^3\text{ cm}^{-1}$ ); HR-MALDI-FT-ICR-MS:  $m/z$  calcd for  $\text{C}_{120}\text{H}_{154}\text{B}_4\text{F}_8\text{N}_{12}\text{O}_4\text{S}_8$ : 2280.0278 [ $M^+$ ]; found: 2280.0281.

**Synthesis of 11:** Compound **11** was synthesized under similar reaction conditions to **4** from 3,6-bis-(4-(2-ethylhexyloxy)phenyl)-2,5-dihydropyrrolyl[3,4-c]pyrrole-1,4-dione (**DPP-4**, 109 mg, 0.18 mmol), 2-aminopyridine (169 mg, 1.8 mmol),  $\text{TiCl}_4$  (0.20 mL, 1.8 mmol), triethylamine (1.0 mL, 7.2 mmol), and  $\text{BF}_3\cdot\text{OEt}_2$  (1.0 mL, 8.1 mmol). The reaction mixture was purified by alumina gel chromatography using  $\text{CHCl}_3$  as an eluent, to give **11** as a blue powder (27 mg, 17%).  $^1\text{H NMR}$  (500 MHz,  $\text{CDCl}_3$ ):  $\delta$  = 8.44 (d,  $J$  = 6.9 Hz, 4H), 8.22 (d,  $J$  = 6.6 Hz, 2H), 7.79 (dd,  $J_1 = J_2 = 7.8$  Hz, 2H), 7.06–7.03 (m, 6H), 3.97 (d,  $J$  = 4.0 Hz, 4H), 1.78–1.34 (m, 18H), 0.98–0.92 ppm (m, 12H); UV/Vis ( $\text{CHCl}_3$ ):  $\lambda_{\text{max}}$  ( $\epsilon$ ) = 316 (23 000), 414 (28 000), 591 (36 000), 638 nm ( $83\,000\text{ mol}^{-1}\text{ dm}^3\text{ cm}^{-1}$ ); HR-MALDI-FT-ICR-MS:  $m/z$  calcd for  $\text{C}_{44}\text{H}_{50}\text{B}_2\text{F}_4\text{N}_6$ : 792.4112 [ $M^+$ ]; found: 792.4113.

## Acknowledgements

This work was partly supported by a Grant-in-Aid for Scientific Research on Innovative Area, "New Polymeric Materials Based on Element-Blocks (No. 25102503), from the Ministry of Education, Culture, Sports, Science, and Technology (MEXT) and a Grant-in-Aid for Young Scientists A (No. 26708003) from Japan Society for the Promotion of Science (JSPS). The authors thank Prof. Takeaki Iwamoto and Dr. Shintaro Ishida, Tohoku University for the X-ray measurement.

**Keywords:** chromophores · density functional calculations · fluorescence spectroscopy · fluorescent probes · UV/Vis spectroscopy

- a) R. P. Haugland, *Handbook of Fluorescent Probes and Research Products*, 9th ed., Molecular Probes, Eugene, **2002**; b) E. U. Akkaya in *Chemosensors of Ion and Molecular Recognition* (Eds.: J.-P. Desvergne, A. W. Czarnik), Kluwer Academic, Dordrecht, **1997**.
- a) P. Bäuerle in *Electronic Materials: The Oligomer Approach* (Eds.: K. Müllen, G. Wegner), Wiley-VCH, Weinheim, **1998**; b) A. R. Murphy, J. M. Fréchet, *Chem. Rev.* **2007**, *107*, 1066–1096; c) Y. Shirota, H. Kageyama, *Chem. Rev.* **2007**, *107*, 953–1010; d) J. Zaumseil, H. Sirringhaus, *Chem. Rev.* **2007**, *107*, 1296–1323.
- D. G. Farnum, G. Mehta, G. G. I. Moore, F. P. Siegal, *Tetrahedron Lett.* **1974**, *15*, 2549–2552.
- a) Z. M. Hao, A. Iqbal, *Chem. Soc. Rev.* **1997**, *26*, 203–213; b) A. Iqbal, M. Jost, R. Kirchmayr, J. Pfenninger, A. Rochat, O. Wallquist, *Bull. Soc. Chim. Belg.* **1988**, *97*, 615–644; c) J. S. Zambounis, Z. Hao, A. Iqbal, *Nature* **1997**, *388*, 131–132.
- O. Wallquist in *High Performance Pigments* (Ed.: H. M. Smith), Wiley-VCH, Weinheim, **2002**, Chapter 11, pp. 159–184.
- a) M. M. Wienk, M. Turbiez, J. Gilot, R. A. Janssen, *J. Adv. Mater.* **2008**, *20*, 2556–2560; b) J. C. Bijleveld, V. S. Gevaerts, D. Di Nuzzo, M. Turbiez, S. G. Mathijssen, D. M. de Leeuw, M. M. Wienk, R. A. Janssen, *Adv. Mater.* **2010**, *22*, E242–246; c) K. H. Hendriks, G. H. Heintges, V. S. Gevaerts, M. M. Wienk, R. A. Janssen, *Angew. Chem.* **2013**, *125*, 8499–8502; *Angew. Chem. Int. Ed.* **2013**, *52*, 8341–8344; d) W. Li, A. Furlan, K. H. Hendriks, M. M. Wienk, R. A. Janssen, *J. Am. Chem. Soc.* **2013**, *135*, 5529–5532; e) W. Li, K. H. Hendriks, A. Furlan, W. S. Roelofs, M. M. Wienk, R. A. Janssen, *J. Am. Chem. Soc.* **2013**, *135*, 18942–18948; f) W. Li, A. Furlan, W. S. Roelofs, K. H. Hendriks, G. W. van Pruissen, M. M. Wienk, R. A. Janssen, *Chem. Commun.* **2014**, *50*, 679–681; g) W. Li, K. H. Hendriks, A. Furlan, W. S. Roelofs, S. C. Meskers, M. M. Wienk, R. A. Janssen, *Adv. Mater.* **2014**, *26*, 1565–1570.
- Recently, new chromophores were synthesized from DPP using reactivity of the pyrrolopyrrole nitrogen atoms; a) A. Janiga, M. Krzeszewski, D. T. Gryko, *Chem. Asian J.* **2015**, *10*, 212–218; b) M. Grzybowski, E. Glodkowska-Mrowka, T. Stoklosa, D. T. Gryko, *Org. Lett.* **2012**, *14*, 2670–2673; c) W. Yue, S. L. Suraru, D. Bialas, M. Muller, F. Würthner, *Angew. Chem.* **2014**, *126*, 6273–6276; *Angew. Chem. Int. Ed.* **2014**, *53*, 6159–6162.
- a) G. M. Fischer, A. R. Ehlers, A. Zumbusch, E. Daltrizzo, *Angew. Chem.* **2007**, *119*, 3824–3827; *Angew. Chem. Int. Ed.* **2007**, *46*, 3750–3753; b) M. Y. Berezin, W. J. Akers, K. Guo, G. M. Fischer, E. Daltrizzo, A. Zumbusch, S. Achilefu, *Biophys. J.* **2009**, *97*, L22–L24; c) G. M. Fischer, M. Isomäki-Kron Dahl, I. Göttker-Schnetmann, E. Daltrizzo, A. Zumbusch, *Chem. Eur. J.* **2009**, *15*, 4857–4864; d) G. M. Fischer, C. Jungst, M. Isomäki-Kron Dahl, D. Gauss, H. M. Möller, E. Daltrizzo, A. Zumbusch, *Chem. Commun.* **2010**, *46*, 5289–5291; e) W. J. Akers, C. Kim, M. Berezin, K. Guo, R. Fuhrhop, G. M. Lanza, G. M. Fischer, E. Daltrizzo, A. Zumbusch, X. Cai, L. V. Wang, S. Achilefu, *ACS Nano* **2011**, *5*, 173–182; f) G. M. Fischer, E. Daltrizzo, A. Zumbusch, *Angew. Chem.* **2011**, *123*, 1442–1445; *Angew. Chem. Int. Ed.* **2011**, *50*, 1406–1409; g) G. M. Fischer, M. K. Klein, E. Daltrizzo, A. Zumbusch, *Eur. J. Org. Chem.* **2011**, 3421–3429; h) S. Wiktorowski, G. M. Fischer, M. J. Winterhalder, E. Daltrizzo, A. Zumbusch, *Phys. Chem. Chem. Phys.* **2012**, *14*, 2921–2928.
- S. Shimizu, T. Iino, Y. Araki, N. Kobayashi, *Chem. Commun.* **2013**, *49*, 1621–1623.
- Recently, Zumbusch et al. reported the synthesis of PPAB using the  $\text{POCl}_3$ -activation method. T. Marks, E. Daltrizzo, A. Zumbusch, *Chem. Eur. J.* **2014**, *20*, 6494–6504.
- A. Saeki, S. Yoshikawa, M. Tsuji, Y. Koizumi, M. Ide, C. Vijayakumar, S. Seki, *J. Am. Chem. Soc.* **2012**, *134*, 19035–19042.
- S. Luňák Jr., J. Vyuňchal, M. Vala, L. Havel, R. Hrdina, *Dyes Pigm.* **2009**, *82*, 102–108.
- C. H. Woo, P. M. Beaujuge, T. W. Holcombe, O. P. Lee, J. M. Fréchet, *J. Am. Chem. Soc.* **2010**, *132*, 15547–15549.
- a) G. E. Ficken, J. D. Kendall, *J. Chem. Soc.* **1960**, 1537–1541; b) N. P. Vasilenko, F. A. Mikhailenko, *Ukr. Khim. Zh.* **1986**, *52*, 308.
- K. Matsumura, M. Ono, H. Kimura, M. Ueda, Y. Nakamoto, K. Togashi, Y. Okamoto, M. Ihara, R. Takahashi, H. Saji, *ACS Med. Chem. Lett.* **2012**, *3*, 58–62.
- a) H. K. Hall, A. B. Padias, P. A. Williams, J. M. Gosau, H. W. Boone, D. K. Park, *Macromolecules* **1995**, *28*, 1–8; b) G. Nawn, S. R. Oakley, M. B. Majewski, R. McDonald, B. O. Patrick, R. G. Hicks, *Chem. Sci.* **2013**, *4*, 612–621.
- M. Kirkus, L. Wang, S. Mothy, D. Beljonne, J. Cornil, R. A. Janssen, S. C. Meskers, *J. Phys. Chem. A* **2012**, *116*, 7927–7936.
- T. Ishiyama, M. Murata, N. Miyaura, *J. Org. Chem.* **1995**, *60*, 7508–7510.
- a) K. L. Billingsley, T. E. Barder, S. L. Buchwald, *Angew. Chem.* **2007**, *119*, 5455–5459; *Angew. Chem. Int. Ed.* **2007**, *46*, 5359–5363; b) T. Ishiyama, Y. Itoh, T. Kitano, N. Miyaura, *Tetrahedron Lett.* **1997**, *38*, 3447–3450; c) T. Ishiyama, K. Ishida, N. Miyaura, *Tetrahedron* **2001**, *57*, 9813–9816.
- F. Odobel, S. Suresh, E. Blart, Y. Nicolas, J.-P. Quintard, P. Janvier, J.-Y. Le Questel, B. Illien, D. Rondeau, P. Richomme, T. Häupl, S. Wallin, L. Hammarström, *Chem. Eur. J.* **2002**, *8*, 3027–3046.
- A. Saeki, Y. Koizumi, T. Aida, S. Seki, *Acc. Chem. Res.* **2012**, *45*, 1193–1202.
- F. C. Grozema, L. D. A. Siebbeles, *J. Phys. Chem. Lett.* **2011**, *2*, 2951–2958.
- T. J. Savenije, J. E. Kroeze, X. Yang, J. Loos, *Adv. Funct. Mater.* **2005**, *15*, 1260–1266.
- A. M. Nardes, A. J. Ferguson, J. B. Whitaker, B. W. Larson, R. E. Larsen, K. Maturová, P. A. Graf, O. V. Boltalina, S. H. Strauss, N. Kopidakis, *Adv. Funct. Mater.* **2012**, *22*, 4115–4127.
- W. Zhang, W. Jin, T. Fukushima, A. Saeki, S. Seki, T. Aida, *Science* **2011**, *334*, 340–343.
- A. J. Ferguson, N. Kopidakis, S. E. Shaheen, G. Rumbles, *J. Phys. Chem. C* **2011**, *115*, 23134–23148.
- A. Saeki, M. Tsuji, S. Seki, *Adv. Energy Mater.* **2011**, *1*, 661–669.
- A. Saeki, M. Tsuji, S. Yoshikawa, A. Gopal, S. Seki, *J. Mater. Chem. A* **2014**, *2*, 6075–6080.
- G. Sheldrick, *Acta Crystallogr. Sect. A* **2008**, *64*, 112–122.
- Yadokari-XG, Software for Crystal Structure Analyses, Wakita, K. (2001); Release of Software (Yadokari-XG 2009) for Crystal Structure Analyses, C. Kabuto, S. Akine, T. Nemoto, E. Kwon, *J. Cryst. Soc. Jpn.* **2009**, *51*, 218–224.

[31] Gaussian 09, Revision A.02, M. J. Frisch, G. W. Trucks, H. B. Schlegel, G. E. Scuseria, M. A. Robb, J. R. Cheeseman, G. Scalmani, V. Barone, B. Men-  
nucci, G. A. Petersson, H. Nakatsuji, M. Caricato, X. Li, H. P. Hratchian,  
A. F. Izmaylov, J. Bloino, G. Zheng, J. L. Sonnenberg, M. Hada, M. Ehara,  
K. Toyota, R. Fukuda, J. Hasegawa, M. Ishida, T. Nakajima, Y. Honda, O.  
Kitao, H. Nakai, T. Vreven, J. A. Montgomery, Jr., J. E. Peralta, F. Ogliaro,  
M. Bearpark, J. J. Heyd, E. Brothers, K. N. Kudin, V. N. Staroverov, R. Ko-  
bayashi, J. Normand, K. Raghavachari, A. Rendell, J. C. Burant, S. S. Iyen-  
gar, J. Tomasi, M. Cossi, N. Rega, J. M. Millam, M. Klene, J. E. Knox, J. B.

Cross, V. Bakken, C. Adamo, J. Jaramillo, R. Gomperts, R. E. Stratmann,  
O. Yazyev, A. J. Austin, R. Cammi, C. Pomelli, J. W. Ochterski, R. L. Martin,  
K. Morokuma, V. G. Zakrzewski, G. A. Voth, P. Salvador, J. J. Dannenberg,  
S. Dapprich, A. D. Daniels, O. Farkas, J. B. Foresman, J. V. Ortiz, J. Cio-  
slowski, D. J. Fox, Gaussian, Inc., Wallingford CT, 2009.

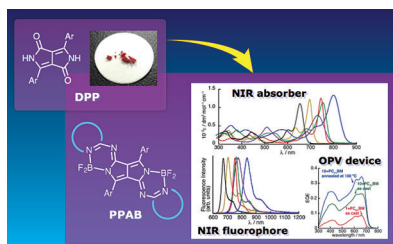
---

Received: October 21, 2014

Published online on ■ ■ ■, 2014

## FULL PAPER

**Fluorescence under control:** The rational control of the absorption and fluorescence of pyrrolopyrrole *aza*-BODIPY (PPAB) molecules in the visible and near infrared regions and panchromatic absorption of the PPAB dimer were achieved (see figure). In addition, application of PPAB molecules as optoelectronic materials was investigated for the first time.



### Fluorescence

*S. Shimizu,\* T. Iino, A. Saeki,\* S. Seki, N. Kobayashi\**



**Rational Molecular Design towards Vis/NIR Absorption and Fluorescence by using Pyrrolopyrrole *aza*-BODIPY and its Highly Conjugated Structures for Organic Photovoltaics**

